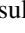





**Femtosecond photoluminescence from monolayer MoS<sub>2</sub>: Time-domain study on exciton diffusion**Kensuke Saito,<sup>1</sup> Mitsuhiro Okada ,<sup>2,\*</sup> Ryo Kitaura ,<sup>2</sup> Hideo Kishida ,<sup>1</sup> and Takeshi Koyama <sup>1,†</sup><sup>1</sup>*Department of Applied Physics, Nagoya University, Nagoya 464–8603, Japan*<sup>2</sup>*Department of Chemistry, Nagoya University, Nagoya 464–8602, Japan*

(Received 1 March 2021; revised 16 April 2021; accepted 20 April 2021; published 3 May 2021)

Transition metal dichalcogenides are expected to be used in transparent, flexible, and highly efficient light-emitting devices. Exciton diffusion is a key factor in device applications. In this study, we measured the photoluminescence (PL) decay of excitons in a MoS<sub>2</sub> monolayer synthesized by chemical vapor deposition on a sapphire substrate. The PL decay of A and B excitons in the femtosecond regime was observed. The PL decay curves were analyzed based on a model of exciton trapping at the deactivation center via diffusion, and the diffusion time until trapping was obtained. The diffusion coefficient and the corresponding exciton mobility were also determined. This study demonstrates the two-dimensional exciton diffusion in the femtosecond regime in the MoS<sub>2</sub> monolayer.

DOI: [10.1103/PhysRevB.103.L201401](https://doi.org/10.1103/PhysRevB.103.L201401)

Transition metal dichalcogenide (TMD) monolayers such as MoS<sub>2</sub>, WS<sub>2</sub>, MoSe<sub>2</sub>, and WSe<sub>2</sub> monolayers emit bright luminescence in the visible and near-infrared spectral regions [1–4]. Owing to their subnanometer thickness and high luminescence efficiency achieved by chemical processes [5], TMDs are expected to be used in transparent, flexible, highly efficient light-emitting devices. For example, a recent paper demonstrated a transparent 3 mm × 2 mm-scale electroluminescence device using WSe<sub>2</sub> monolayer [6]. Another light-emitting device utilizing the photoluminescence (PL) of interlayer excitons in a heterostructure of WSe<sub>2</sub> and MoS<sub>2</sub> has been developed [7]. In this device, the diffusion of excitons photoexcited in an excitation spatial region to an emission region is controlled by applying an out-of-plane voltage to the intermediate region, and switching of luminescence is enabled. Therefore, it is important to understand the two-dimensional diffusion of excitons in TMDs for device applications. The exciton diffusion in WS<sub>2</sub> [8–10], WSe<sub>2</sub> [11], and MoSe<sub>2</sub> [12] has been studied, and very recently, the exciton diffusion in exfoliated monolayer MoS<sub>2</sub> on a SiO<sub>2</sub>/Si substrate was studied by measuring the spatial expansion of the light-emitting region from a point irradiated by laser light [13]. However, a time-domain study on exciton diffusion in monolayer MoS<sub>2</sub> has not been conducted yet.

For light-emitting devices, a strong steady-state luminescence from the material is desired. A key parameter governing the intensity of steady-state luminescence is the nonradiative decay time of excitons. One of the sources for this decay is trapping at a deactivation center, for example, a defect, via diffusive motion. Some defects are inactivated by filling with excitons and/or charges generated by photoexcitation, and residual excitons are not trapped at the filled defects and

survive a relatively long time [14]. This can be one of reasons for excitation density dependence of the exciton mobility in the steady-state measurements and time-resolved measurements with modest time resolutions. In contrast, time-resolved measurements with sufficiently high time resolutions enable us to directly observe the diffusion and trapping dynamic of excitons till the filling of the defects. The exciton decay time in monolayer MoS<sub>2</sub> has been widely investigated by femtosecond pump-probe measurements [15–19]. In a typical analysis of the pump-probe measurements [15], the recovery of an exciton absorption band after femtosecond pump-pulse irradiation was fitted to a multiexponential function model, and the fast component with a time constant of ~3 ps was attributed to the exciton trapping at defects. In general, bleaching of an exciton absorption band is caused by the excitation of excitons as well as electrons and holes. Hence, it is difficult to obtain pure exciton decay from the recovery of the absorption band. In contrast, in time-resolved PL measurements, exciton decay is predominantly observed because the excitonic PL is much stronger than that of free electron-hole pairs owing to the much higher oscillator strength of the excitons.

Among the excitonic states, steady-state luminescence is mainly emitted from the energetically lowest state. In TMD monolayers, the degeneracies of two highest valence bands and two lowest conduction bands are lifted at the *K* point by the spin-orbit coupling, and two exciton states, A and B exciton states, appear [20]. Hence, PL of the energetically lower A exciton is relatively strong in the steady-state measurements [1,2]. Analysis of the steady-state PL intensities of A and B excitons has been done assuming the decay time of the B excitons to the A exciton state to be ~1 ps [21]. For a direct detection of decay of the B excitons, femtosecond time-resolved PL measurement is expected.

To the best of the authors' knowledge, the shortest time resolution of reported time-resolved PL measurements was 0.8 ps for MoSe<sub>2</sub> and WSe<sub>2</sub> monolayers [22] and about 4 ps for MoS<sub>2</sub> monolayer [23,24], which was achieved by using a streak camera. In the case of MoS<sub>2</sub> monolayer, the PL

\*Present address: Nanomaterials Research Institute, National Institute of Advanced Industrial Science and Technology (AIST), Tsukuba, Ibaraki 305–8565, Japan.

†Corresponding author: [koyama@nuap.nagoya-u.ac.jp](mailto:koyama@nuap.nagoya-u.ac.jp)

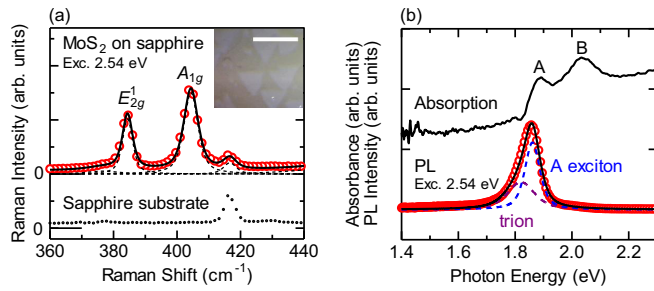


FIG. 1. (a) Raman scattering spectra of MoS<sub>2</sub> sample (circles) and sapphire substrate (dotted curve). Solid curve shows the result of curve fitting using four Voigt functions (dashed curves). Inset shows optical microscope image of the sample (scale bar: 100  $\mu\text{m}$ ). (b) Absorption (black curve) and steady-state PL spectra (circles) of MoS<sub>2</sub> sample. Solid curve shows the result of curve fitting using two Voigt functions (dashed curves) for A exciton and trion.

decay with two components was observed, and the fast decay component was comparable to or less than the time resolution. For direct observation of exciton decay within a few picoseconds, PL measurement with femtosecond time resolution is required.

In the present study, femtosecond time-resolved PL measurements were conducted to observe the two-dimensional diffusion of excitons and obtain the exciton diffusion coefficient in monolayer MoS<sub>2</sub>. Single crystals of monolayer MoS<sub>2</sub> were synthesized on a sapphire substrate by chemical vapor deposition (CVD). The inset in Fig. 1(a) depicts a typical optical microscope image of the sample. The bright white triangles show single crystals of monolayer MoS<sub>2</sub>. The lengths of the triangle edges were  $\sim 60 \mu\text{m}$ . It is known that monolayer MoS<sub>2</sub> on sapphire is in the *n*-doped state [25]. The absorption spectrum of a single crystal was measured using a spectrophotometer with a microscope (Jasco MSV-5200). The aperture size was 30  $\mu\text{m}$ . Steady-state PL and Raman scattering spectra were measured using a micro-Raman spectrometer (Renishaw inVia). A 50 $\times$  objective lens was used, and the spot size on the sample was 2  $\mu\text{m}$ . The excitation light source was a diode laser with a wavelength of 488 nm (corresponding photon energy is 2.54 eV), and the excitation density was  $9 \times 10^6 \text{ W m}^{-2}$ . The spectral resolution was 1.3  $\text{cm}^{-1}$ . Time-resolved PL measurements were carried out using the frequency up-conversion technique [26–28]. The light source was a mode-locked Ti:sapphire laser (82 MHz, 800 nm, 90 fs). The second harmonic light of the output of the laser was generated in a  $\beta$ -barium borate crystal and used as an excitation pulse (400 nm, corresponding photon energy is 3.10 eV). Residual fundamental light was used as the gate pulse. The excitation pulse was focused on a sample with a spot size of 50  $\mu\text{m}$ . The instrument response function (Gaussian shape, full width at half maximum (FWHM) of 200 fs) was determined by measuring the cross-correlation trace between the gate and excitation pulses. All measurements were conducted at 300 K in an air atmosphere. It is noted that PL from the sapphire substrate was not observed in the steady-state and time-resolved PL measurements.

We evaluated the number of MoS<sub>2</sub> layers in the sample using Raman scattering spectroscopy. Figure 1(a) shows a typical Raman scattering spectrum of the sample excited at

2.54 eV (488 nm). For comparison, the spectrum of the sapphire substrate is shown with a dotted line. Peaks at 385 and 404  $\text{cm}^{-1}$  in the spectrum are assigned to the  $E_{2g}^1$  and  $A_{1g}$  phonon modes, respectively [29]. We measured the spectra at randomly selected 10 points involving other crystals on the sapphire substrate, so that we obtained the averaged information on the MoS<sub>2</sub> monolayers synthesized in this study. The average values of the peak positions of the  $E_{2g}^1$  and  $A_{1g}$  phonon modes are 384.6 and 404.4  $\text{cm}^{-1}$ , respectively, and the difference between them is 19.8  $\text{cm}^{-1}$ . A previous study showed that the difference in Raman shift between the  $E_{2g}^1$  and  $A_{1g}$  peak positions for the CVD-grown monolayer MoS<sub>2</sub> is 19.6–20.6  $\text{cm}^{-1}$  [30]. Therefore, the number of MoS<sub>2</sub> layers in the sample was determined to be one.

We further tested the number of layers using steady-state PL spectroscopy. Figure 1(b) shows the absorption and PL spectra of the sample. The absorption bands at 1.89 and 2.03 eV are attributed to A and B exciton absorptions, respectively [1,2]. The PL spectrum was observed with photoexcitation at 2.54 eV. A broad asymmetric PL peak at 1.86 eV is observed (details of the spectral decomposition are provided later), while a previous study showed that the PL spectrum of multilayer MoS<sub>2</sub> involve a PL band around 1.5 eV assigned to indirect transitions other than PL bands of neutral and charged excitons [31]. Thus, the PL spectrum in Fig. 1(b) supports that our sample is a monolayer MoS<sub>2</sub>.

The PL spectrum was analyzed by using two pseudo-Voigt functions, referring to the literature [32]. The PL peak at 1.86 eV is decomposed into PL bands of A exciton and negative trion, which are shown as dashed curves in Fig. 1(b). The spectral weight ratio of the negative trion to the A exciton bands is 0.77. The trion spectral weight defined by the spectral weight ratio of the trion to the sum of the trion and exciton [33] is  $0.77/(0.77 + 1) = 0.44$ . The trion spectral weight calculated by using Eqs. (S5) and (S6) and shown in Fig. 4(b) in Ref. [33] indicates that this value corresponds to the rate of 0.1  $\text{ps}^{-1}$  for formation of the trions from the excitons. The inverse value is 10 ps, which is the time constant of the trion-to-exciton decay. It is noteworthy that a PL band of the B exciton in the steady-state measurement is not observed, suggesting that the decay time of B excitons is much shorter than that of A excitons. On the other hand, in the femtosecond time-resolved PL measurements, we observed PL signals at not only 1.89, but also 2.03 eV, which correspond to the decay behaviors of A and B excitons, respectively. At the photon energy of 1.89 eV, the tail of the PL band of trion is overlapped with the A-exciton PL band. Because the exciton binding energy of several hundreds of eV is one order of magnitude larger than the trion binding energy [33], the oscillator strength of the exciton is much larger than that of the trion. The PL in the femtosecond time window is instantaneous emission compared to the steady-state PL and is sensitive to the oscillator strength. Hence, in the femtosecond time-resolved PL measurements, the observed PL at 1.89 eV is mainly due to A excitons.

Figures 2(a) and 2(b) show the PL decay curves at 2.03 and 1.89 eV (B and A exciton bands), respectively. The excitation photon energy was 3.10 eV, and the excitation density was  $8 \mu\text{J cm}^{-2}$  per pulse (the corresponding photon flux is  $4 \times 10^{16}$  photons  $\text{m}^{-2}$  per pulse). This photon energy is situated

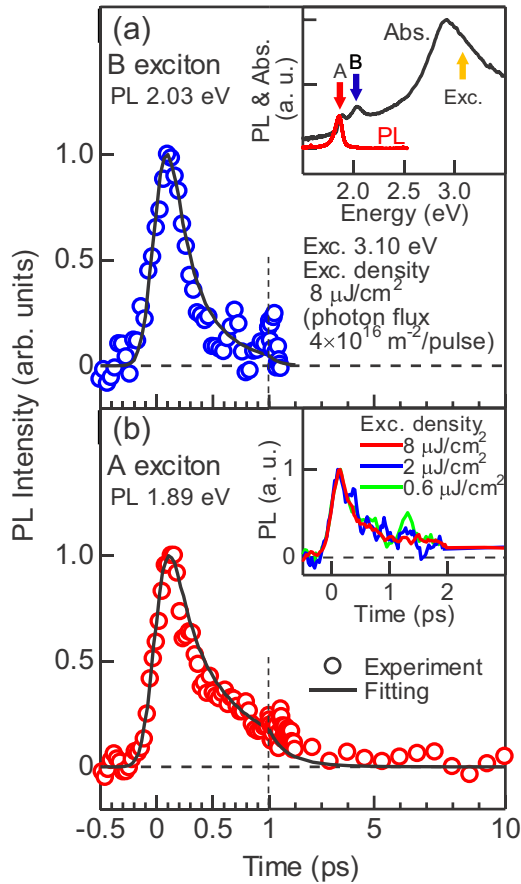


FIG. 2. PL decay curves of monolayer MoS<sub>2</sub> sample at (a) 2.03 eV (B exciton band) and (b) 1.89 eV (A exciton band). The excitation photon energy was 3.10 eV, and excitation density was 8 μJ cm<sup>-2</sup> per pulse (corresponding photon flux is 4 × 10<sup>16</sup> photons m<sup>-2</sup> per pulse). Circles and solid curves indicate results of the experiment and fitting analysis. Insets in (a) and (b) show absorption and PL spectra and excitation density dependence of PL decay of the A exciton, respectively.

in an absorption band assigned to band-nested interband transitions along the  $\Gamma$ - $K$  line in the Brillouin zone [34]. The excitation and probe photon energies are indicated in the absorption band plotted in the inset of Fig. 2(a). The PL of the B exciton almost completely decays within 1.5 ps. The PL of the A exciton shows a similar fast decay, but a long-lived weak component is observed. These decay behaviors support the steady-state PL spectrum shown in the inset of Fig. 2(a), which involves a strong A exciton band and an undetectable B exciton band. Note that neither decay curve can be reproduced by a single-exponential function. In particular, the decay curve of the A exciton can be reproduced using a multiexponential function model or stretched exponential function model.

If exciton-exciton annihilation occurs, the decay in the early time region becomes fast with an increase in the excitation density [15,35,36], which makes it possible to reproduce the PL decay curve using multiexponential functions or stretched exponential function. The inset in Fig. 2(b) shows the excitation density dependence of the PL decay of the A exciton. This figure shows no dependence of the PL decay on the excitation density up to 8 μJ cm<sup>-2</sup> per pulse, which is

consistent with the literature [37]. Hence, the PL decay behavior cannot be explained by the exciton-exciton annihilation.

The PL decay curves were analyzed using a model describing the trapping of excited species at a deactivation center via diffusion, as schematically depicted in Fig. 3. An excitation pulse with a photon energy of 3.10 eV generates electron-hole pairs, and A and B excitons are quickly formed [Fig. 3(a)]. The B excitons [Fig. 3(b)] decay due to (i) trapping at defects via diffusion, (ii) relaxation to the A exciton state, (iii) relaxation to the trion state, or (iv) other processes involving radiative recombination and multiphonon emission by exciton-phonon scattering. The A excitons [Fig. 3(c)] are further generated by B-to-A exciton relaxation, and they decay due to (i) trapping at defects via diffusion, (ii) relaxation to the trion state, or (iii) other processes as above. The time dependence of the number of excitons decaying by defect trapping via diffusion is expressed by stretched exponential function  $\propto \exp[-(t/\tau_d)^\beta]$  [38,39], where the parameters  $\beta$  and  $\tau_d$  are given later. Involving this decay term, other decay terms [21,33], and generation term, the rate equations of the concentrations of A and B excitons,  $n_A$  and  $n_B$ , are given by

$$\begin{aligned} \frac{dn_A}{dt} &= G_A - \frac{\beta}{\tau_d} \left(\frac{t}{\tau_d}\right)^{\beta-1} n_A + \frac{n_B}{\tau_{BA}} - \frac{n_A}{\tau_{trion}} - \frac{n_A}{\tau_A}, \\ \frac{dn_B}{dt} &= G_B - \frac{\beta}{\tau_d} \left(\frac{t}{\tau_d}\right)^{\beta-1} n_B - \frac{n_B}{\tau_{BA}} - \frac{n_B}{\tau_{trion}} - \frac{n_B}{\tau_B}. \end{aligned}$$

Here,  $G_A$  and  $G_B$  are generation functions of A and B excitons. We assume that both excitons are formed equally and quickly [40] by absorption of the excitation pulse, and the  $G_A$  and  $G_B$  shapes are taken as the excitation pulse shape.  $\beta$  is a parameter that depends on the dimensionality of diffusion, which is set to 1/3, 1/2, and 3/5 for one-, two-, and three-dimensional diffusion, respectively. Because monolayer MoS<sub>2</sub> is a two-dimensional material, excitons diffuse two dimensionally. In fact, the spatial mapping of PL from excitons in monolayer MoS<sub>2</sub> shows isotropic expansion of the light-emitting region from the laser-excited spot [13]. For this reason,  $\beta$  is set to 1/2.  $\tau_d$  is the characteristic diffusion time until trapping at the deactivation center.  $\tau_{BA}$  is a decay time constant of the B exciton to A exciton state, and the reported value of  $\tau_{BA}$  is 1 ps [21,41].  $\tau_{trion}$  is the time constant of decay to the trion state and is dependent on the doped charge concentration, which is reflected in the PL spectrum [33]. The spectral weight ratio of the trion to the A exciton PL band is 0.77, which corresponds to a  $\tau_{trion}$  of 10 ps.  $\tau_A$  and  $\tau_B$  are decay time constants of A and B excitons, except for trapping at the deactivation center and decay to the trion state. The possible sources of these time constants are radiative decay and decay by exciton-phonon scattering. The reported radiative decay time is 10 ns [42], and the decay time by exciton-phonon scattering is 50 ps at room temperature [43]. Because these time constants are much larger than the observed PL decay, the last terms in the above equations are neglected. The free parameter in curve fitting was  $\tau_d$ . The PL decay curves in Fig. 2 were well reproduced when  $\tau_d = 0.09 \pm 0.01$  ps.

For the two-dimensional diffusion, the diffusion coefficient ( $D$ ) was estimated by  $1/\tau_d = 12\pi Dn_D$ , where  $n_D$  is the areal concentration of deactivation centers, i.e., defect



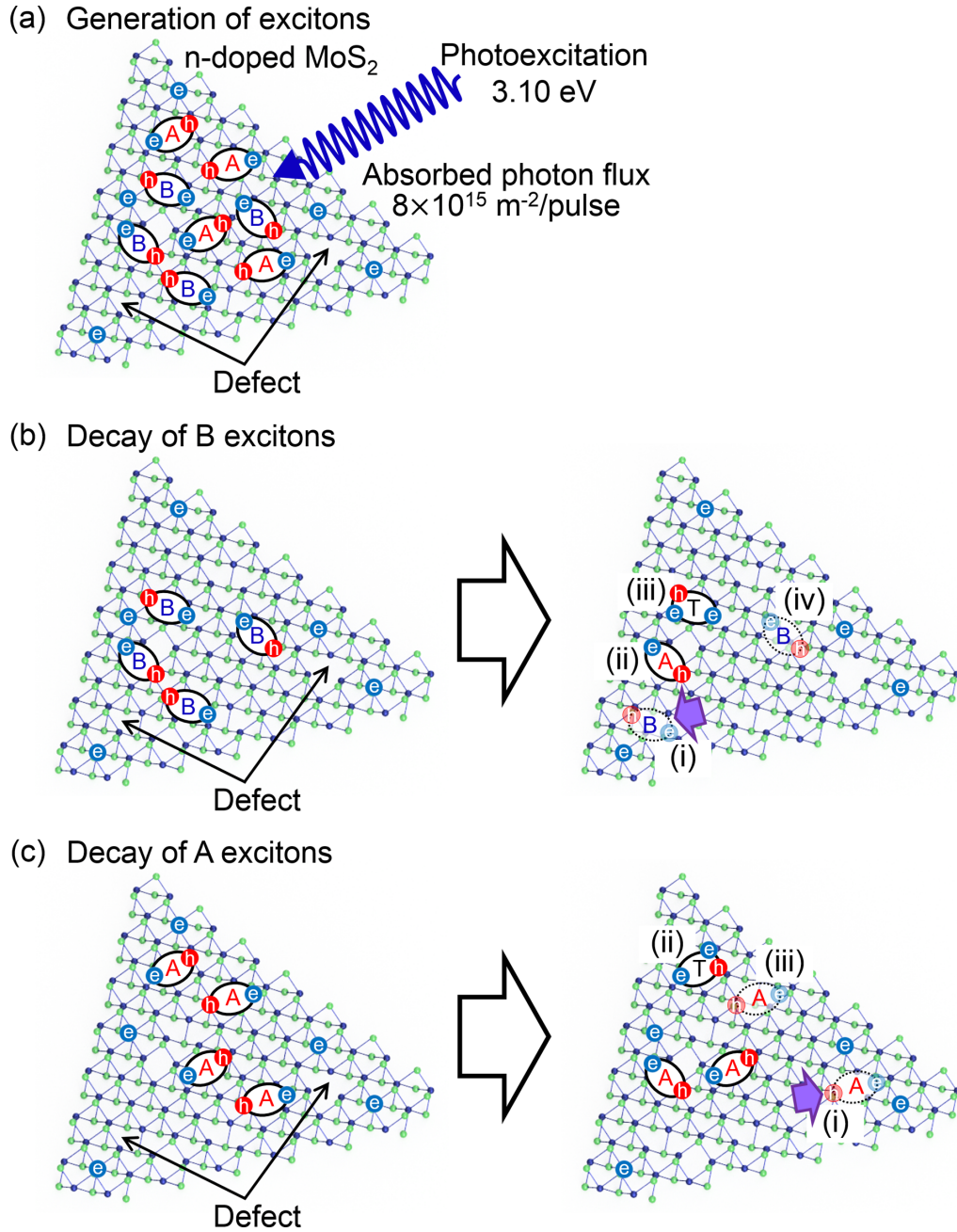


FIG. 3. Schematic illustrations of exciton generation and decay. (a) Generation of excitons by an excitation pulse with a photon energy of 3.10 eV. The energy density of the excitation pulse was  $8 \mu\text{J cm}^{-2}$  per pulse (corresponding photon flux is  $4 \times 10^{16}$  photons  $\text{m}^{-2}$  per pulse), and the absorbed photon flux was  $8 \times 10^{15}$  photons  $\text{m}^{-2}$  per pulse. (b) Decay of B excitons. The B excitons decay due to (i) trapping at defects via diffusion, (ii) relaxation to the A exciton state, (iii) relaxation to the trion state, or (iv) other processes involving radiative recombination and multiphonon emission. (c) Decay of A excitons. The A excitons decay due to (i) trapping at defects via diffusion, (ii) relaxation to the trion state, or (iii) other processes. The B-to-A exciton relaxation generates A excitons.

concentration [38]. The defect concentration can be estimated from the widths of the  $E_{2g}^1$  and  $A_{1g}$  phonon modes [44]. The average FWHM value of the  $E_{2g}^1$  mode in the measured spectra is  $3.92 \text{ cm}^{-1}$ . The corresponding defect concentration is  $(4 \pm 1) \times 10^{12} \text{ cm}^{-2}$ , which is consistent with the estimation using the peak width of the  $A_{1g}$  mode (average value  $5.42 \text{ cm}^{-1}$ ). Using the values of  $\tau_d$  ( $0.09 \pm 0.01 \text{ ps}$ ) and  $n_D$  [ $(4 \pm 1) \times 10^{12} \text{ cm}^{-2}$ ], the lower bound of  $D$  was estimated to be  $0.07 \pm 0.02 \text{ cm}^2 \text{ s}^{-1}$ , if we assume that the trapping

probability at the defect is unity. Taking the temperature  $T$  to be 300 K, the exciton mobility  $\mu (= eD/k_B T)$  was estimated to be  $3 \pm 1 \text{ cm}^2 \text{ V}^{-1} \text{ s}^{-1}$ , where  $e$  is the elementary charge and  $k_B$  is the Boltzmann constant.

Finally, we discuss the obtained exciton mobility in comparison to the carrier mobility. The carrier mobility in CVD-grown monolayer MoS<sub>2</sub> has been investigated for various crystal sizes and various substrates [45–48]. Because there is a positive correlation between the crystal size and defect

concentration in the CVD-grown monolayer MoS<sub>2</sub> [49], we choose the carrier mobility of  $0.3\text{--}5\text{ cm}^2\text{ V}^{-1}\text{ s}^{-1}$  in the CVD-grown monolayer MoS<sub>2</sub> with the same size as our sample [50]. The mobility is inversely proportional to the mass of the particle [51]. The effective masses of electrons and holes in monolayer MoS<sub>2</sub> are  $0.35m_0$  and  $0.45m_0$ , respectively, where  $m_0$  represents the electron rest mass [52]. Hence, the exciton translational mass is  $0.8m_0$ . For carrier and exciton mobilities limited by defect trapping, the carrier mobility of  $0.3\text{--}5\text{ cm}^2\text{ V}^{-1}\text{ s}^{-1}$  in the previous study is converted to the exciton mobility of  $0.13\text{--}2.2\text{ cm}^2\text{ V}^{-1}\text{ s}^{-1}$ . This value is smaller than that of  $3 \pm 1\text{ cm}^2\text{ V}^{-1}\text{ s}^{-1}$  obtained in the present study. The carrier is subject to long-range scattering by doped charges and charged impurities [53], and the carrier mobility might be lower than that of the exciton, the charge of which is neutral. In fact, it has been pointed out that the neutral exciton mobility can be higher than the carrier mobility owing to weak interactions with charged impurities and piezoelectric phonons in monolayer MoSe<sub>2</sub> [54].

In summary, we carried out absorption, steady-state, and time-resolved PL, and Raman scattering measurements for the monolayer MoS<sub>2</sub> CVD grown on a sapphire substrate. The fitting analysis of PL decay curves of A and B excitons enabled us to obtain the diffusion time of excitons until trapping at deactivation centers via two-dimensional diffusion. The characteristic diffusion time was  $0.09 \pm 0.01$  ps. The defect concentration was estimated to be  $(4 \pm 1) \times 10^{12}\text{ cm}^{-2}$  from the widths of the  $E_{2g}^1$  and  $A_{1g}$  phonon modes. Using these values, we determined the value of the diffusion coefficient to be  $0.07 \pm 0.02\text{ cm}^2\text{ s}^{-1}$ , and the corresponding exciton mobility as  $3 \pm 1\text{ cm}^2\text{ V}^{-1}\text{ s}^{-1}$  at 300 K. This study demonstrated the two-dimensional exciton diffusion in the femtosecond regime observed through ultrafast time-resolved PL measurements. Our results advance the understanding of exciton diffusion in two-dimensional materials.

This work was supported by JSPS KAKENHI Grants No. JP26107520 and No. JP16H00908.

- 
- [1] A. Splendiani, L. Sun, Y. Zhang, T. Li, J. Kim, C.-Y. Chim, G. Galli, and F. Wang, Emerging photoluminescence in monolayer MoS<sub>2</sub>, *Nano Lett.* **10**, 1271 (2010).
- [2] K. F. Mak, C. Lee, J. Hone, J. Shan, and T. F. Heinz, Atomically Thin MoS<sub>2</sub>: A New Direct-Gap Semiconductor, *Phys. Rev. Lett.* **105**, 136805 (2010).
- [3] S. Tongay, J. Zhou, C. Ataca, K. Lo, T. S. Matthews, J. Li, J. C. Grossman, and J. Wu, Thermally driven crossover from indirect toward direct bandgap in 2D semiconductors: MoSe<sub>2</sub> versus MoS<sub>2</sub>, *Nano Lett.* **12**, 5576 (2012).
- [4] H. Zeng, G.-B. Liu, J. Dai, Y. Yan, B. Zhu, R. He, L. Xie, S. Xu, X. Chen, W. Yao, and X. Cui, Optical signature of symmetry variations and spin-valley coupling in atomically thin tungsten dichalcogenides, *Sci. Rep.* **3**, 1608 (2013).
- [5] M. Amani, D.-H. Lien, D. Kiriya, J. Xiao, A. Azcatl, J. Noh, S. R. Madhupathy, R. Addou, S. KC, M. Dubey, K. Cho, R. M. Wallace, S.-C. Lee, J.-H. He, J. W. Ager III, X. Zhang, E. Yablonovitch, and A. Javey, Near-unity photoluminescence quantum yield in MoS<sub>2</sub>, *Science* **350**, 1065 (2015).
- [6] D.-H. Lien, M. Amani, S. B. Desai, G. H. Ahn, K. Han, J.-H. He, J. W. Ager III, M. C. Wu, and A. Javey, Large-area and bright pulsed electroluminescence in monolayer semiconductors, *Nat. Commun.* **9**, 1229 (2018).
- [7] D. Unuchek, A. Ciarrocchi, A. Avsar, K. Watanabe, T. Taniguchi, and A. Kis, Room-temperature electrical control of exciton flux in a van der Waals heterostructure, *Nature (London)* **560**, 340 (2018).
- [8] T. Kato and T. Kaneko, Transport dynamics of neutral excitons and trions in monolayer WS<sub>2</sub>, *ACS Nano* **10**, 9687 (2016).
- [9] M. Kulig, J. Zipfel, P. Nagler, S. Blanter, C. Schüller, T. Korn, N. Paradiso, M. M. Glazov, and A. Chernikov, Exciton Diffusion and Halo Effects in Monolayer Semiconductors, *Phys. Rev. Lett.* **120**, 207401 (2018).
- [10] J. Zipfel, M. Kulig, R. Perea-Causín, S. Brem, J. D. Ziegler, R. Rosati, T. Taniguchi, K. Watanabe, M. M. Glazov, E. Malic, and A. Chernikov, Exciton diffusion in monolayer semiconductors with suppressed disorder, *Phys. Rev. B* **101**, 115430 (2020).
- [11] F. Cadiz, C. Robert, E. Courtade, M. Manca, L. Martinelli, T. Taniguchi, K. Watanabe, T. Amand, A. C. H. Rowe, D. Paget, B. Urbaszek, and X. Marie, Exciton diffusion in WSe<sub>2</sub> monolayers embedded in a van der Waals heterostructure, *Appl. Phys. Lett.* **112**, 152106 (2018).
- [12] T. Hotta, S. Higuchi, A. Ueda, K. Shinokita, Y. Miyauchi, K. Matsuda, K. Ueno, T. Taniguchi, K. Watanabe, and R. Kitaura, Exciton diffusion in hBN-encapsulated monolayer MoSe<sub>2</sub>, *Phys. Rev. B* **102**, 115424 (2020).
- [13] S. Z. Uddin, H. Kim, M. Lorenzon, M. Yeh, D.-H. Lien, E. S. Barnard, H. Htoon, A. Weber-Bargioni, and A. Javey, Neutral exciton diffusion in monolayer MoS<sub>2</sub>, *ACS Nano* **14**, 13433 (2020).
- [14] S. D. Stranks, V. M. Burlakov, T. Leijtens, J. M. Ball, A. Goriely, and H. J. Snaith, Recombination Kinetics in Organic-Inorganic Perovskites: Excitons, Free Charge, and Subgap States, *Phys. Rev. Appl.* **2**, 034007 (2014).
- [15] H. Shi, R. Yan, S. Bertolazzi, J. Brivio, B. Gao, A. Kis, D. Jena, H. G. Xing, and L. Huang, Exciton dynamics in suspended monolayer and few-layer MoS<sub>2</sub> 2D crystals, *ACS Nano* **7**, 1072 (2013).
- [16] Q. Wang, S. Ge, X. Li, J. Qiu, Y. Ji, J. Feng, and D. Sun, Valley carrier dynamics in monolayer molybdenum disulfide from helicity-resolved ultrafast pump-probe spectroscopy, *ACS Nano* **7**, 11087 (2013).
- [17] Z. Nie, R. Long, L. Sun, C.-C. Huang, J. Zhang, Q. Xiong, D. W. Hewak, Z. Shen, O. V. Prezhdo, and Z.-H. Loh, Ultrafast carrier thermalization and cooling dynamics in few-layer MoS<sub>2</sub>, *ACS Nano* **8**, 10931 (2014).
- [18] H. Wang, C. Zhang, and F. Rana, Ultrafast dynamics of defect-assisted electron-hole recombination in monolayer MoS<sub>2</sub>, *Nano Lett.* **15**, 339 (2015).
- [19] E. A. A. Pogna, M. Marsili, D. D. Fazio, S. D. Conte, C. Manzoni, D. Sangalli, D. Yoon, A. Lombardo, A. C. Ferrari, A. Marini, G. Cerullo, and D. Prezzi, Photo-induced bandgap renormalization governs the ultrafast response of single-layer MoS<sub>2</sub>, *ACS Nano* **10**, 1182 (2016).

- [20] A. Kormányos, G. Burkard, M. Gmitra, J. Fabian, V. Zólyomi, N. D. Drummond, and V. Fal'ko, k-p theory for two-dimensional transition metal dichalcogenide semiconductors, *2D Mater.* **2**, 022001 (2015).
- [21] K. M. McCreary, A. T. Hanbicki, S. V. Sivaram, and B. T. Jonker, A- and B-exciton photoluminescence intensity ratio as a measure of sample quality for transition metal dichalcogenide monolayers, *APL Mater.* **6**, 111106 (2018).
- [22] C. Robert, D. Lagarde, F. Cadiz, G. Wang, B. Lassagne, T. Amand, A. Balocchi, P. Renucci, S. Tongay, B. Urbaszek, and X. Marie, Exciton radiative lifetime in transition metal dichalcogenide monolayers, *Phys. Rev. B* **93**, 205423 (2016).
- [23] D. Lagarde, L. Bouet, X. Marie, C. R. Zhu, B. L. Liu, T. Amand, P. H. Tan, and B. Urbaszek, Carrier and Polarization Dynamics in Monolayer MoS<sub>2</sub>, *Phys. Rev. Lett.* **112**, 047401 (2014).
- [24] F. Cadiz, S. Tricard, M. Gay, D. Lagarde, G. Wang, C. Robert, P. Renucci, B. Urbaszek, and X. Marie, Well separated trion and neutral excitons on superacid treated MoS<sub>2</sub> monolayers, *Appl. Phys. Lett.* **108**, 251106 (2016).
- [25] W. H. Chae, J. D. Cain, E. D. Hanson, A. A. Murthy, and V. P. Dravid, Substrate-induced strain and charge doping in CVD-grown monolayer MoS<sub>2</sub>, *Appl. Phys. Lett.* **111**, 143106 (2017).
- [26] T. Koyama, Y. Miyata, K. Asaka, H. Shinohara, Y. Saito, and A. Nakamura, Ultrafast energy transfer of one-dimensional excitons between carbon nanotubes: A femtosecond time-resolved luminescence study, *Phys. Chem. Chem. Phys.* **14**, 1070 (2012).
- [27] T. Koyama, Y. Ito, K. Yoshida, M. Tsuji, H. Ago, H. Kishida, and A. Nakamura, Near-infrared photoluminescence in the femtosecond time region in monolayer graphene on SiO<sub>2</sub>, *ACS Nano* **7**, 2335 (2013).
- [28] H. Imaeda, T. Koyama, H. Kishida, K. Kawahara, H. Ago, R. Sakakibara, W. Norimatsu, T. Terasawa, J. Bao, and M. Kusunoki, Acceleration of photocarrier relaxation in graphene achieved by epitaxial growth: Ultrafast photoluminescence decay of monolayer graphene on SiC, *J. Phys. Chem. C* **122**, 19273 (2018).
- [29] H. Li, Q. Zhang, C. C. R. Yap, B. K. Tay, T. H. T. Edwin, A. Olivier, and D. Baillargeat, From bulk to monolayer MoS<sub>2</sub>: Evolution of Raman scattering, *Adv. Funct. Mater.* **22**, 1385 (2012).
- [30] J. Jeon, S. K. Jang, S. M. Jeon, G. Yoo, Y. H. Jang, J.-H. Park, and S. Lee, Layer-controlled CVD growth of large-area two-dimensional MoS<sub>2</sub> films, *Nanoscale* **7**, 1688 (2015).
- [31] K. Liu, L. Zhang, T. Cao, C. Jin, D. Qiu, Q. Zhou, A. Zettl, P. Yang, S. G. Louie, and F. Wang, Evolution of interlayer coupling in twisted molybdenum disulfide bilayers, *Nat. Commun.* **5**, 4966 (2014).
- [32] D. Kaplan, Y. Gong, K. Mills, V. Swaminathan, P. M. Ajayan, S. Shirodkar, and E. Kaxiras, Excitation intensity dependence of photoluminescence from monolayers of MoS<sub>2</sub> and WS<sub>2</sub>/MoS<sub>2</sub> heterostructures, *2D Mater.* **3**, 015005 (2016).
- [33] S. Mouri, Y. Miyauchi, and K. Matsuda, Tunable photoluminescence of monolayer MoS<sub>2</sub> via chemical doping, *Nano Lett.* **13**, 5944 (2013).
- [34] P. D. Cunningham, K. M. McCreary, A. T. Hanbicki, M. Currie, B. T. Jonker, and L. M. Hayden, Charge trapping and exciton dynamics in large-area CVD grown MoS<sub>2</sub>, *J. Phys. Chem. C* **120**, 5819 (2016).
- [35] D. Sun, Y. Rao, G. A. Reider, G. Chen, Y. You, L. Brézín, A. R. Harutyunyan, and T. F. Heinz, Observation of rapid exciton–exciton annihilation in monolayer molybdenum disulfide, *Nano Lett.* **14**, 5625 (2014).
- [36] L. Yuan and L. Huang, Exciton dynamics and annihilation in WS<sub>2</sub> 2D semiconductors, *Nanoscale* **7**, 7402 (2015).
- [37] Y. Yu, Y. Yu, C. Xu, A. Barrette, K. Gundogdu, and L. Cao, Fundamental limits of exciton-exciton annihilation for light emission in transition metal dichalcogenide monolayers, *Phys. Rev. B* **93**, 201111(R) (2016).
- [38] B. Ya. Balagurov and V. G. Vaks, Random walks of a particle on lattices with traps, *Sov. Phys. JETP* **38**, 968 (1974).
- [39] T. Koyama, A. Nakamura, and H. Kishida, Microscopic mobility of polarons in chemically doped polythiophenes measured by employing photoluminescence spectroscopy, *ACS Photonics* **1**, 655 (2014).
- [40] C. Trovatiello, F. Katsch, N. J. Borys, M. Selig, K. Yao, R. Borrego-Varillas, F. Scotognella, I. Kriegel, A. Yan, A. Zettl, P. J. Schuck, A. Knorr, G. Cerullo, and S. D. Conte, The ultrafast onset of exciton formation in 2D semiconductors, *Nat. Commun.* **11**, 5277 (2020).
- [41] S. Cha, J. H. Sung, S. Sim, J. Park, H. Heo, M.-H. Jo, and H. Choi, Is-intraexcitonic dynamics in monolayer MoS<sub>2</sub> probed by ultrafast mid-infrared spectroscopy, *Nat. Commun.* **7**, 10768 (2016).
- [42] X. Gan, Y. Gao, K. F. Mak, X. Yao, R.-J. Shiue, A. van der Zande, M. E. Trusheim, F. Hatami, T. F. Heinz, J. Hone, and D. Englund, Controlling the spontaneous emission rate of monolayer MoS<sub>2</sub> in a photonic crystal nanocavity, *Appl. Phys. Lett.* **103**, 181119 (2013).
- [43] T. Korn, S. Heydrich, M. Hirmer, J. Schmutzler, and C. Schüller, Low-temperature photocarrier dynamics in monolayer MoS<sub>2</sub>, *Appl. Phys. Lett.* **99**, 102109 (2011).
- [44] S. Mignuzzi, A. J. Pollard, N. Bonini, B. Brennan, I. S. Gilmore, M. A. Pimenta, D. Richards, and D. Roy, Effect of disorder on Raman scattering of single-layer MoS<sub>2</sub>, *Phys. Rev. B* **91**, 195411 (2015).
- [45] Y.-H. Lee, X.-Q. Zhang, W. Zhang, M.-T. Chang, C.-T. Lin, K.-D. Chang, Y.-C. Yu, J. T.-W. Wang, C.-S. Chang, L.-J. Li, and T.-W. Lin, Synthesis of large-area MoS<sub>2</sub> atomic layers with chemical vapor deposition, *Adv. Mater.* **24**, 2320 (2012).
- [46] H. Liu, M. Si, S. Najmaei, A. T. Neal, Y. Du, P. M. Ajayan, J. Lou, and P. D. Ye, Statistical study of deep submicron dual-gated field-effect transistors on monolayer chemical vapor deposition molybdenum disulfide films, *Nano Lett.* **13**, 2640 (2013).
- [47] H. Schmidt, S. Wang, L. Chu, M. Toh, R. Kumar, W. Zhao, A. H. C. Neto, J. Martin, S. Adam, B. Özyilmaz, and G. Eda, Transport properties of monolayer MoS<sub>2</sub> grown by chemical vapor deposition, *Nano Lett.* **14**, 1909 (2014).
- [48] D. Dumcenco, D. Ovchinnikov, K. Marinov, P. Lazić, M. Gibertini, N. Marzari, O. L. Sanchez, Y.-C. Kung, D. Krasnozhan, M.-W. Chen, S. Bertolazzi, P. Gillet, A. F. Morral, A. Radenovic, and A. Kis, Large-area epitaxial monolayer MoS<sub>2</sub>, *ACS Nano* **9**, 4611 (2015).
- [49] Z. G. Yu, Y.-W. Zhang, and B. I. Yakobson, An anomalous formation pathway for dislocation-sulfur vacancy complexes in polycrystalline monolayer MoS<sub>2</sub>, *Nano Lett.* **15**, 6855 (2015).
- [50] N. Huo, Y. Yang, Y.-N. Wu, X.-G. Zhang, S. T. Pantelides, and G. Konstantatos, High carrier mobility in monolayer

- CVD-grown MoS<sub>2</sub> through phonon suppression, [Nanoscale \*\*10\*\*, 15071 \(2018\)](#).
- [51] O. L. Berman, R. Ya. Kezerashvili, and Y. E. Lozovik, Spin Hall effect for polaritons in a transition metal dichalcogenide embedded in a microcavity, [Phys. Rev. B \*\*99\*\*, 085438 \(2019\)](#).
- [52] V. Shahnazaryan, O. Kyriienko, and H. Rostami, Exciton routing in the heterostructure of a transition metal dichalcogenide monolayer on a paraelectric substrate, [Phys. Rev. B \*\*100\*\*, 165303 \(2019\)](#).
- [53] N. Ma and D. Jena, Charge Scattering and Mobility in Atomically Thin Semiconductors, [Phys. Rev. X \*\*4\*\*, 011043 \(2014\)](#).
- [54] N. Kumar, Q. Cui, F. Ceballos, D. He, Y. Wang, and H. Zhao, Exciton diffusion in monolayer and bulk MoSe<sub>2</sub>, [Nanoscale \*\*6\*\*, 4915 \(2014\)](#).